












RESEARCH ARTICLE | JULY 23 2025

Symmetry progression and band vs Mott character of CdPS₃ under pressure

Sambridhi Shah ; Seongjae Choi ; Kevin A. Smith ; Yanhong Gu ; Brian Taylor ; Matthew Cothrine ; David Mandrus ; Zhenxian Liu ; Heung-Sik Kim ; Janice L. Musfeldt  



APL Mater. 13, 071127 (2025)

<https://doi.org/10.1063/5.0274796>

 CHORUS



Articles You May Be Interested In

A study of the efficiency of “intelligent shells”


Phys. Plasmas (January 1998)

Effect of smoothing by spectral dispersion on flow induced laser beam deflection: The random phase modulation scheme

Phys. Plasmas (March 1998)

Parametric instabilities due to relativistic electron mass variation

Phys. Plasmas (February 1998)



**Your One-Stop Shop for the
Best Brands in Optics**

- Extensive inventory with over 34,000 products available & 2,900 new products
- Fast shipping from our 9 distribution centres around the globe
- Bringing 80+ years of optical expertise to customers worldwide

Edmund
optics | worldwide

Shop Now

Symmetry progression and band vs Mott character of CdPS₃ under pressure

Cite as: APL Mater. 13, 071127 (2025); doi: 10.1063/5.0274796

Submitted: 8 April 2025 • Accepted: 8 July 2025 •

Published Online: 23 July 2025



Sambridhi Shah,¹ Seongjae Choi,² Kevin A. Smith,¹ Yanhong Gu,¹ Brian Taylor,¹
Matthew Cothrine,³ David Mandrus,^{3,4,5} Zhenxian Liu,⁶ Heung-Sik Kim,^{2,a)}
and Janice L. Musfeldt^{1,4,b)}

AFFILIATIONS

¹ Department of Chemistry, University of Tennessee, Knoxville, Tennessee 37996, USA

² Department of Semiconductor Physics and Institute of Quantum Convergence Technology, Kangwon National University, Chuncheon, Gangwon-do, South Korea

³ Materials Science and Engineering Department, University of Tennessee, Knoxville, Tennessee 37996, USA

⁴ Department of Physics and Astronomy, University of Tennessee, Knoxville, Tennessee 37996, USA

⁵ Materials Science and Technology Division, Oak Ridge National Laboratory, Oak Ridge, Tennessee 37831, USA

⁶ Department of Physics, University of Illinois Chicago, Chicago, Illinois 60607-7059, USA

a) heungsikim@kangwon.ac.kr

b) Author to whom correspondence should be addressed: musfeldt@tennessee.edu

ABSTRACT

Complex chalcogenides are renowned for their tunable electronic, magnetic, and optical properties under external stimuli. The MPX₃ family ($M = \text{Mn, Ni, Co, V}$; $X = \text{S, Se}$) is a platform for many exciting discoveries—especially under compression—although CdPS₃ is thought to be different because the Cd center possesses a filled 4d shell, which precludes Mottness. Here, we combine synchrotron-based infrared absorbance and Raman scattering spectroscopies with diamond anvil cell techniques, complementary lattice dynamics calculations, and an analysis of the energy landscape to reveal a series of structural phase transitions in CdPS₃. We find four distinct pressure-driven transitions, with low frequency modes detectable over the full 35 GPa range of our investigation. A group–subgroup analysis along with our first-principles calculations allows us to partially unravel the space group sequence. For instance, the first critical pressure is a monoclinic $C2/m$ to trigonal $R\bar{3}$ transition at 10 GPa. Despite the softness and overall sensitivity to pressure, we do not locate an insulator-to-metal transition in this pressure range, indicating that the energy scale for gap closure is significantly higher than expected. We discuss these findings in terms of force-induced color change and Mott vs band character in this system.

© 2025 Author(s). All article content, except where otherwise noted, is licensed under a Creative Commons Attribution (CC BY) license (<https://creativecommons.org/licenses/by/4.0/>). <https://doi.org/10.1063/5.0274796>

I. INTRODUCTION

Among the family of van der Waals magnets, antiferromagnetic insulators with chemical formula MPX₃ ($M = \text{Mn, Ni, Co, V, Cd}$; $X = \text{S, Se}$) are attracting considerable attention.^{1–4} In addition to natural chemical tunability,^{5,6} these materials are sensitive to external stimuli such as magnetic field,^{7–11} pressure,^{12–15} strain,¹⁶ and light,^{17,18} as well as layer number via exfoliation.^{19,20} Compression is extraordinarily effective for manipulating properties because in addition to controlling bond lengths and angles, it modifies the van der Waals gap and the c/a ratio.^{21–24} This gives rise to a number

of distinctive qualities including layer sliding, insulator-to-metal transitions, magnetic dimensionality crossovers, superconductivity, piezochromism, and the possibility of polar metal and orbital-selective Mott states.^{24–28} From the structural point of view, these systems comprise [P₂S₆]^{4–} dimers, with transition metal centers forming a honeycomb lattice around the dimers.^{29,30} Despite the common structural building blocks, no two of the MPX₃ materials host the same sequence of transitions or properties under compression, suggesting that each is more singular than previously supposed.³ As the nonmagnetic analog in this set of compounds, CdPS₃ is especially under-explored.^{31–35} An important consequence

of the filled $4d$ orbitals in this system is that Mottness^{25,36,37} may be inhibited in favor of band-like character. At the same time, there are continuing questions about how to grow stoichiometric CdPS_3 , the true nature and sequence of the high pressure transitions, and overall structural stability that the current literature has been unable to resolve.^{33,34} We therefore decided to revisit the high pressure vibrational properties of CdPS_3 with special emphasis on the role of filled Cd^{2+} $4d$ orbitals and the structure–property relations that can be unraveled in this class of materials.

In this work, we combine synchrotron-based infrared absorbance and Raman scattering spectroscopies with diamond anvil cell techniques and complementary first-principles calculations to uncover the series of structural phase transitions in CdPS_3 . Analysis of the phonon behavior under compression reveals critical pressures at 10, 18, 29, and 33 GPa—all of which take place without triggering an insulator–metal transition. Comparison with predicted mode trends allows us to unravel the monoclinic $C2/m \rightarrow R\bar{3}$ symmetry crossover at $P_{C,1} = 10$ GPa. Although the $R\bar{3}$ space group is not a direct super-group of $C2/m$, the van der Waals gap is unusually wide in this system, which may allow related structures with the same number of atoms/unit cell to become stable. At the same time, we find that the energy scale for bandgap closure is significantly higher than expected. We discuss blocking of the insulator-to-metal transition in terms of screening of the charging energy U (which makes the on-site Coulomb interactions irrelevant) and the large van der Waals gap. The rate of bandgap closure is sensitive to these effects as well: -30 meV/GPa in CdPS_3 vs -50 meV/GPa in MnPS_3 .²⁷ The difference is presumably due to enhanced Coulomb interactions in the Mn analog.

II. METHODS

A. Synthesis and characterization of CdPS_3

High quality single crystals of CdPS_3 were grown via chemical vapor transport.³⁸ Stoichiometric amounts of Cd (Thermo Scientific, 99.99% purity), P (Alfa Aesar, 99.999% purity, metals basis), and S (Alfa Aesar, 99.9995% purity, metals basis), totaling ~ 3.2 g, were homogenized in an argon-filled glovebox. The resulting mixture was then transferred into a silica ampoule along with 0.035 g of iodine (I_2). The ampoule was subsequently sealed under vacuum. The synthesis was conducted in a one-zone tube furnace, set to a temperature of 650°C with a heating rate of $2^\circ\text{C}/\text{min}$. Using the natural gradient of the furnace, a temperature difference of $\sim 60^\circ\text{C}$ between the hot and cold ends of the ampoule was maintained for 8 days. Following the synthesis, the furnace was allowed to cool to room temperature. Single crystals were obtained at the “cold” end of the ampoule, appearing as predominantly transparent, colorless flakes with a slight yellow tinge observed in some clusters. After the synthesis, x-ray diffraction was performed using Cu $K\alpha$ radiation with $\lambda = 1.540598$ Å using an Empyrean instrument (40 mA, 45 kV). The sample was prepared by grinding to a fine powder and placing the material on a low-background silicon sample holder to minimize background interference. X-ray diffraction peaks for the restricted hkl indices for the $C2/m$ space group were obtained by Rietveld refinement. The x-ray diffraction analysis is presented in the [supplementary material](#). This verifies the quality of our crystals.³⁹

B. Loading the diamond anvil cell for high-pressure measurements

To study high pressure phases in CdPS_3 , we loaded a carefully selected crystal into a symmetric diamond anvil cell from Jade Corporation. The cell had type 2as diamonds and $400\text{ }\mu\text{m}$ culets. We used a stainless steel gasket with a hole size of $100\text{ }\mu\text{m}$ and a thickness of $\sim 60\text{ }\mu\text{m}$. Along with the sample, a pressure medium and an annealed ruby ball were also loaded. We employed both KBr and petroleum jelly as the pressure medium depending upon the measurement. Proper selection of the pressure-transmitting medium ensured that the pressure distribution across the sample was quasi-hydrostatic. The fluorescence of the ruby ball was used for pressure determination as shown in Fig. S2 of the [supplementary material](#).^{40,41} Additional detail is available in the [supplementary material](#).

C. Vibrational spectroscopies

We performed accelerator-based infrared spectroscopy using the 22-IR-1 beamline at the National Synchrotron Light Source II at Brookhaven National Laboratory. Experiments were carried out in transmittance mode over the $50\text{--}750\text{ cm}^{-1}$ range, employing a Bruker 80v Fourier transform infrared spectrometer and bolometer or MCT detector. The spectral resolution was 4 cm^{-1} . Raman scattering measurements were performed in the back-scattering geometry on a Horiba LabRAM HR Evolution Raman spectrometer over the $0\text{--}750\text{ cm}^{-1}$ frequency range. We used an excitation wavelength of 532 nm, a power of 0.15 mW, an 1800 lines per mm grating, and a liquid nitrogen-cooled CCD detector. To enhance the signal/noise ratio, we integrated for 10 sec and averaged three times.

D. Symmetry analysis

We carried out a group–subgroup analysis using our analysis of frequency vs pressure trends along with the Bilbao Crystallographic Server.⁴² We used the appearance and disappearance of different phonons and the symmetry operations that they represent to move up and down the symmetry tree and to determine the symmetry progression. At the same time, we tested a number of space groups that have been seen in related van der Waals materials.³ Candidates were examined by calculating their energies relative to other candidates under those conditions, relaxing the structure to one with a suitable match to the experiment and comparing the calculated lattice dynamics of that candidate structure to our experimental results.

E. Lattice dynamics calculations

Density functional theory calculations were carried out using the projector-augmented-wave (PAW) method as implemented in Vienna *Ab initio* Simulation Package (VASP).^{43,44} A revision of the Perdew–Burke–Ernzerhof generalized gradient approximation for solids (PBEsol) was chosen as the exchange–correlation functional.⁴⁵ For comparison, a revised Strongly Constrained and Appropriately Normed (r2SCAN) semilocal functional⁴⁶ and the Heyd–Scuseria–Ernzerhof (HSE06) hybrid functional⁴⁷ were employed. We employed gamma-centered k -meshes where the number of the k -grid points along the direction of each reciprocal lattice vector multiplied by the corresponding Bravais lattice vector (in Å) is close to 50. For all self-consistent calculations,

plane wave energy cutoff and energy convergence criterion were set to 500 and 10^{-8} eV, respectively. Internal atomic coordinates were relaxed until Hellmann–Feynman force on each atom satisfies convergence criteria, 10^{-4} eV/Å. To compute infrared and Raman-active modes of vibration, we employed the PHONOPY code interfaced with VASP.^{48,49} The mode-decomposed phonon frequencies were calculated as a function of pressure to compare with the experimental phonon frequencies.

III. RESULTS AND DISCUSSION

A. CdPS₃ under ambient conditions: Vibrational modes, symmetry assignments, and crystal quality

Figures 1(a) and 1(b) display the vibrational properties of CdPS₃ under ambient conditions. We assign the Raman and infrared spectral features based upon group theory and complementary lattice dynamics calculations. For a monoclinic structure in the $C2/m$ space group, group theory predicts 12 infrared-active modes ($5A_u + 7B_u$) and 15 Raman-active modes ($8A_g + 7B_g$).^{42,52,53} We observe nine infrared-active features ($4A_u + 5B_u$) and nine Raman-active phonons ($7A_g + 2B_g$) in our experimental data. Presumably, the others have weak intensities or are in different directions. These symmetries are indicated in Fig. 1 and listed in Tables SI and SII of the [supplementary material](#) alongside experimental and theoretical frequencies and mode displacement patterns. For instance, the lowest frequency B_g mode at 27 cm^{-1} is assigned to buckling of the Cd honeycomb lattice, and the A_g mode near 78 cm^{-1} is the dimerization of Cd atoms along the b -direction of the $C2/m$ unit cell within the honeycomb layers. Taken together, these findings place the mode assignments and overall vibrational pattern of CdPS₃ on a firm foundation.

There are important crystal quality issues to highlight as well. In our hands, CdPS₃ displays two well-defined Raman-active lattice modes near 27 and 78 cm^{-1} , in excellent agreement with our dynamics calculations [Fig. 1(a)]. This is quite different from Refs. 33 and

35, where the lowest frequency mode is absent under ambient conditions. Presumably, this is because the Cd-related phonons are not well developed when stoichiometry is problematic. In fact, the stoichiometry is reported to be $\text{Cd}_{0.89}\text{P}_{0.9}\text{S}_{2.5}$ in Ref. 35. This underscores the synthetic challenge with these materials and demonstrates the importance of well-characterized crystals. Naturally, we performed x-ray diffraction to identify the phase and confirm the quality of our crystals. All observed peaks are attributed to CdPS₃ [Fig. 1(c)], with no additional features detected from other phases (e.g., S, CdS₂, CdO), which are known potential by-products of the growth process. Rietveld refinement yields the best fit for a $C2/m$ crystal structure, consistent with the predicted model. Additional details are available in the [supplementary material](#).

B. Vibrational properties of CdPS₃ under pressure

Figures 2 and 3 summarize the vibrational properties of CdPS₃ as a function of pressure. The ability to bring infrared and Raman scattering techniques together is one of the many distinctive aspects of our work. It allows us to perform a group–subgroup analysis and at least partially unravel the sequence of pressure-driven structural phase transitions in this material.^{42,53} In addition, infrared spectroscopy provides insights into electronic properties such as metallicity, with identifiable characteristics due to the development of a Drude response and phonon screening.⁵⁴ As usual, we identify critical pressures by analyzing the appearance or disappearance of peaks and inflection points in the frequency vs pressure data. The vibrational properties of CdPS₃ are reversible upon pressure release as discussed in the [supplementary material](#).

C. Raman scattering of CdPS₃ under pressure

Figures 2(a) and 2(b) summarize the Raman scattering response of CdPS₃ as a function of pressure. The spectral features are sharp and well-separated, so we can easily track their behavior. We immediately notice that all modes harden under compression.

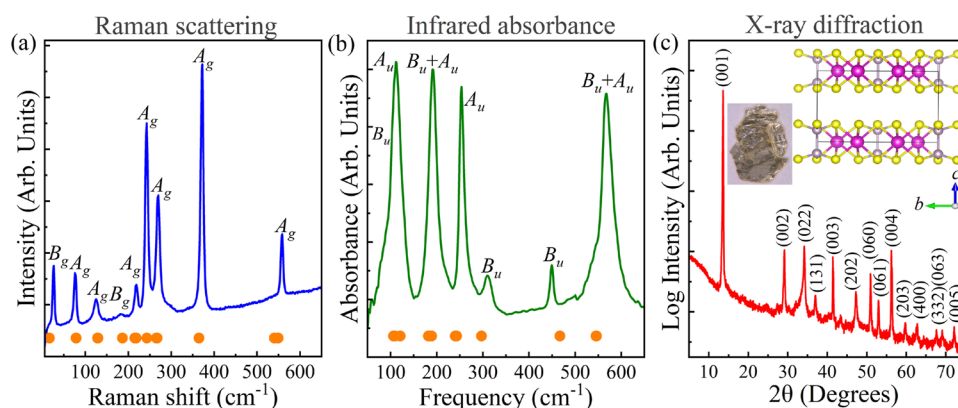


FIG. 1. Crystal structure and vibrational properties of CdPS₃. [(a) and (b)] Raman scattering and infrared absorbance of CdPS₃ under ambient conditions along with the theoretically predicted phonon frequencies for the $C2/m$ space group as orange spheres. The mode symmetries are labeled. (c) X-ray diffraction pattern of powdered CdPS₃, photo of the single crystal, and the $C2/m$ crystal structure,⁵⁰ where Cd, P, and S are indicated using purple, gray, and yellow spheres and visualized using VESTA software.⁵¹ The sheet thickness is 3.89 Å , and the van der Waals gap is 3.95 Å . These values are obtained from a crystal structure analysis. Compared to the other MPS₃ materials, these values are large. As a result, the interlayer binding energy is small, making it easy for layers to slip.

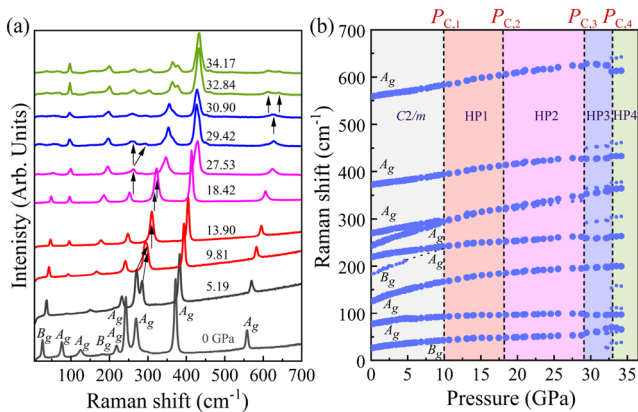


FIG. 2. Raman scattering of CdPS₃ under compression. (a) Raman scattering response as a function of pressure. Only selected curves are shown. A fuller set of data is included in the [supplementary material](#). The pressures are labeled, and arrows indicate features of interest. The spectra associated with the C2/m phase are shown in black, and those in the higher pressure phases are shown in red (HP1), pink (HP2), blue (HP3), and green (HP4), respectively. (b) Frequency vs pressure plot of these data at room temperature. The dashed line near 200 cm⁻¹ in panel (b) guides the eye. The black dashed lines denote critical pressures. Phonon intensity is indicated by the size of the blue symbols.

Two pairs of phonons also condense near 10 GPa. At 18 GPa, we observe the development of a subtle peak near 314 cm⁻¹. Additional features also appear above 29 GPa due to a symmetry reduction. Furthermore, a new peak emerges at 612 cm⁻¹ accompanied by the appearance of several additional phonon modes in the low frequency region near 33 GPa, adding to the complexity in this system under pressure. The development of these additional features suggests an overall reduction in symmetry with increasing pressure. This sequence allows us to define four critical pressures ($P_{C,1} = 10$ GPa, $P_{C,2} = 18$ GPa, $P_{C,3} = 29$ GPa, and $P_{C,4} = 33$ GPa) and five independent phases (C2/m, HP1, HP2, HP3 and HP4).

While the critical pressure at 10 GPa is confirmed by prior Raman scattering measurements and theoretical predictions,^{33,34} our work differs from the literature in several important aspects. In the results of Niu *et al.*, the 80 cm⁻¹ feature disappears by 1.1 GPa, and the 30 cm⁻¹ peak appears only at 1.1 GPa and splits at higher pressure.³³ This is not what we find. Instead, both the lattice modes near 27 and 78 cm⁻¹ are clearly present under ambient conditions and develop systematically across the full pressure range. Of course, they become more challenging to track at higher pressure, but that does not obscure the main point, which is that in high quality samples, the spectra below 100 cm⁻¹ are beautifully simple. We conclude that sample stoichiometry is incredibly important. At the same time, Li *et al.* theoretically predict a transition from monoclinic C2/m to trigonal R $\bar{3}$ at 1.5 GPa.³⁴ In our hands, R $\bar{3}$ is in close proximity to C2/m, but we assign it to the crossover at 10 GPa as discussed below.

D. Infrared properties of CdPS₃ under pressure

Figure 3 summarizes the synchrotron infrared absorbance of CdPS₃ under compression. These measurements reveal four critical pressures and five distinct phases and provide information on

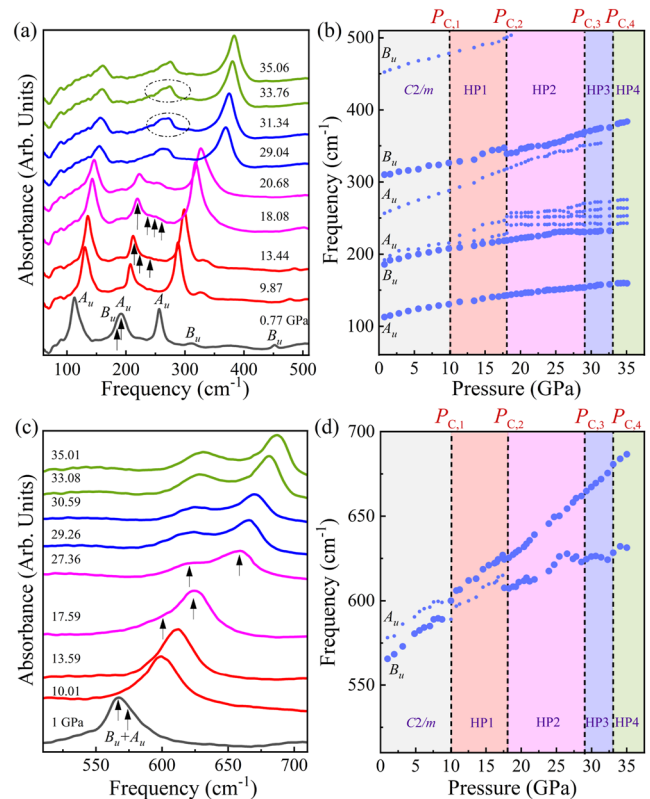


FIG. 3. Infrared absorbance of CdPS₃ under compression. [(a) and (c)] Close-up views of infrared absorbance as a function of pressure. Selected curves are shown to highlight spectral changes. A more complete dataset is provided in the [supplementary material](#). [(b) and (d)] Frequency vs pressure plots for these data at room temperature. Pressures are labeled, and arrows + circles point out features of interest. Due to sensitivity issues, it is difficult to resolve the three phonons near 100 cm⁻¹, so we track only the main peak. The black dashed lines denote critical pressures, and the weak intensity phonons are indicated with small blue circles in panels (b) and (d). Spectra associated with the C2/m phase are shown in black and those for high pressure phases are shown in red (HP1), pink (HP2), blue (HP3), and green (HP4), respectively.

symmetry breaking and restoration involving the odd-symmetry vibrational modes. In addition to subtle slope changes in several modes, $P_{C,1}$ is defined by how the A_u symmetry P-S stretching mode near 578 cm⁻¹ crosses the 565 cm⁻¹ B_u mode. $P_{C,2}$ is indicated by the disappearance of a B_u symmetry mode near 500 cm⁻¹ and the appearance of peaks at 250 and 255 cm⁻¹. The latter are precisely identified by model oscillator fits (using Voigt functions) to resolve the individual peaks and their trends.⁵⁵ Several noticeable intensity changes mark $P_{C,3}$. At $P_{C,4} = 33$ GPa, the 232 cm⁻¹ mode disappears, and the 627 cm⁻¹ peak changes intensity. Therefore, the full sequence of pressure-induced phase transitions in CdPS₃ is verified by our infrared work. A similar complicated sequence of structural phase transitions is observed in NiPS₃,²⁴ but what differentiates CdPS₃ from this system is that the insulator-to-metal transition is absent. In fact, the infrared absorbance spectra of CdPS₃ display no evidence for metallicity under any pressure conditions that we have

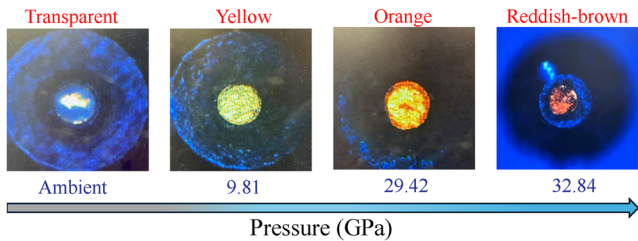


FIG. 4. Color change of CdPS_3 under compression: Photographs of piezochromic CdPS_3 inside the diamond anvil cell at various pressures. The gasket hole in the ambient pressure image is 100 μm in diameter and serves as a relative scale bar. The gasket hole likely expands by a few percent under compression.

explored up to 35 GPa (Fig. 3). The absence of a Drude free carrier response demonstrates that this system does not undergo an insulator-to-metal transition even at 35 GPa. As a reminder, a Drude oscillator is a broad electronic band centered at zero frequency that screens the phonon modes due to developing metallicity. This behavior contrasts with other members of the MPX_3 family, such as CoPS_3 ,⁵⁶ $\text{V}_{0.5}\text{PS}_3$,³⁶ NiPS_3 ,^{13,24} MnPS_3 ,²⁷ FePS_3 ,^{23,57} CrPS_4 ,⁵⁷ and CrPS_3 ⁵⁸ where metallicity has been reported as low as 7 GPa and as high as 23 GPa. We conclude that the heavy Cd^{2+} cation, with its filled 4d orbitals, plays a key role in stabilizing the electronic structure, thereby inhibiting the delocalization of electrons that typically leads to metallization.^{24,27,28,59,60} The material maintains its semiconducting character even up to 35 GPa and as a result reveals a full sequence of structural phase transitions. This resistance to pressure-induced metallization deviates from prior literature,³⁴ which proposed (but did not verify) a transition to a metallic state at 25 GPa. This is why it is so important to measure the infrared—and not just the Raman—response.

We can verify this finding by examining the color properties of CdPS_3 (Fig. 4). The crystals are colorless under ambient conditions, yellow near 10 GPa, orange at 29 GPa, and a reddish-brown near 33 GPa. This suggests that the bandgap remains open (although it is closing gradually) and that the Cd compound does not host a transition to the metallic state under the conditions explored here.⁶¹ Instead, CdPS_3 retains semiconducting character, and the insulator-to-metal transition either (i) takes place at much higher pressures or (ii) is blocked entirely. This is quite different from MnPS_3 , which undergoes a dramatic color change from green \rightarrow yellow \rightarrow red \rightarrow midnight black and systematic reduction of the bandgap (at a rate of ~ 50 meV/GPa) before the gap closes and metallicity emerges at 20 GPa.²⁷ The bandgap appears to drop more slowly in CdPS_3 compared with the Mn and Ni analogs (Fig. S6, supplementary material). As discussed below, this may be a consequence of band vs Mott character in this system.

E. Understanding the structural phase transition at 10 GPa in CdPS_3

We begin by focusing on $P_{C,1}$, which is a transition from monoclinic $C2/m$ to a new higher symmetry state. It is evidenced by the condensation of a pair of Raman-active A_g modes and a pair of $A_g + B_g$ Raman-active features as well as a crossing of the A_u and B_u modes in the infrared. Substantial volume changes have been reported in the vicinity of 10 GPa,^{33,34} and prior Raman scattering

and theoretical work suggest that the system evolves from $C2/m$ to $R\bar{3}$ to trigonal $P\bar{3}1m$ across this pressure range.^{33,34} What differentiates our effort from the earlier work is that we can track the behavior of both even- and odd-symmetry vibrational modes and use the trends to better confirm (or eliminate) certain space group candidates.

We employed the Bilbao server to analyze different symmetry-allowed pathways,^{24,42,52,62} and we applied group–supergroup relationships to identify possible space groups linked to the symmetry changes in CdPS_3 across $P_{C,1}$. This method normally works well because the irreducible representations of different crystal phases fully reflect the symmetry of the entire crystal.^{24,63} The challenge in this case is that the space groups are very close. The analysis yields several candidates including $P\bar{3}1m$, $P2/m$, $Pmmm$, $Fmmm$, and $P6/mmm$. We also considered other space groups that have been observed in the MPS_3 family of complex chalcogenides such as $R\bar{3}$, $P\bar{3}$, $P\bar{3}1m$, and $P3$.^{24,27,57,64} These candidates were further refined by examining the overall number of infrared- and Raman-active vibrational modes expected for each of the supergroups and comparing the results with our spectral data. Two candidates stood out: $P\bar{3}1m$ and $R\bar{3}$. The calculated phonon modes for CdPS_3 in each of these space groups are shown in Fig. S5, supplementary material. Further examination reveals that $R\bar{3}$ provides the superior match. Figure 5 displays the calculated phonon frequencies of CdPS_3 under compression. Note that the trend is the most continuous when assuming the transition point to be $P = 5$ GPa, which is smaller than the experimental critical pressure (10 GPa). Also the lowest B_g mode becomes soft beyond 5 GPa [Fig. 5(a)], unlike what we find in our experiments [Fig. 2(b)]. Such discrepancies may originate from the neglect of long-range force constants.

From a comparison of relaxed structures and computed enthalpies vs pressure of the $C2/m$, $P\bar{3}1m$, and $R\bar{3}$ phases (Fig. S7, supplementary material), we expect that the first pressure-induced structural transition occurring at 10 GPa is from the $C2/m$ to $R\bar{3}$ phases for the following reasons: (i) the slopes of Raman- and infrared-active modes [Figs. 5(a) and 5(b)] remain smoother in $C2/m \rightarrow R\bar{3}$ transition at the critical pressure than those in

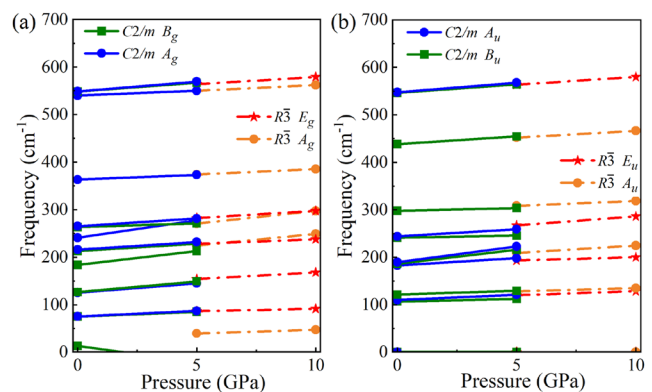


FIG. 5. Computed phonon frequencies of CdPS_3 under compression: phonon frequencies computed via *ab initio* electronic structure calculations as a function of pressure, where (a) Raman- and (b) infrared-active mode are plotted. Note that phonon frequencies from the $C2/m$ and $R\bar{3}$ structure are shown in the pressure intervals of $0 \leq P \leq 5$ and $5 \leq P \leq 10$ GPa, respectively.

TABLE I. Electronic configuration, bandgap, and pressure-driven insulator-to-metal transition of CdPS₃ compared with several members of the MPS₃ family of materials.

Material	Electronic configuration	Bandgap (eV)	P_{IMT} (GPa)	Reference
CdPS ₃	Cd ²⁺ , 4d ¹⁰	3.54	≥35	This work
MnPS ₃	Mn ²⁺ , 3d ⁵	2.64	20	27
FePS ₃	Fe ²⁺ , 3d ⁶	1.5	13.6	57
CoPS ₃	Co ²⁺ , 3d ⁷	1.5	6.7	56
NiPS ₃	Ni ²⁺ , 3d ⁸	1.6	23	24

$C2/m \rightarrow P\bar{3}1m$ and (ii) the presence of the lowest B_g mode located below 50 cm⁻¹ in the experimental Raman spectra [Fig. 2(b)], which should connect to the A_g mode in the $R\bar{3}$ structure beyond the first transition, is completely absent in the $P\bar{3}1m$ phase [Figs. S5(a) and S5(b), [supplementary material](#)]. Hence we conclude that the first transition is likely to be from $C2/m$ to $R\bar{3}$. Our enthalpy calculation [Fig. S7(b), [supplementary material](#)] supports this conclusion and is consistent with other theoretical predictions.^{33,34}

F. CdPS₃ is a band insulator

Since the 4d shell of Cd is completely full (Table I), there do not appear to be strong correlations in CdPS₃ due to the Coulomb repulsion U . We therefore conclude that the system is a band insulator, where the bandgap originates from the energy difference between the fully filled sulfur p - and empty phosphorous p -orbitals (Fig. S8, [supplementary material](#)). Therefore, one can expect that the bandgap in CdPS₃ should be relatively insensitive to external pressure since the gap is mostly determined by the difference between the atomic energy levels, which are marginally affected by the pressure. This scenario is very different from that in Mott-insulating MnPS₃ or NiPS₃, where bandgap closure leads to enhanced screening of the on-site Coulomb repulsion and adds positive feedback to the rate of gap closure, sometimes resulting in sudden gap collapse and a discontinuous transition.^{24,25,27} For instance, the rate of bandgap closure in MnPS₃ is −50 meV/GPa, whereas that in CdPS₃ is approximately −30 meV/GPa [Fig. S6(b), [supplementary material](#)]. The difference can presumably be attributed to enhanced Coulomb interactions in the Mn analog.

IV. SUMMARY

To investigate the symmetry progression and band vs Mott charcater of complex chalcogenides with fully filled 4d orbitals, we measured the synchrotron-infrared absorbance and Raman scattering spectra of CdPS₃ under pressures up to 35 GPa. Our results, combined with symmetry analysis, lattice dynamics calculations, and comparisons with previous studies on the MPS₃ family (where $M = \text{Fe, Co, Ni, Mn}$), reveal a sequence of structural phase transitions in CdPS₃. In particular, we identify four critical pressures at 10, 18, 29, and 33 GPa, corresponding to five distinct structural phases. Group-subgroup analysis and lattice dynamics indicate a symmetry change from monoclinic $C2/m \rightarrow$ trigonal $R\bar{3}$ at 10 GPa. Unlike other MPS₃ compounds, CdPS₃ shows no signs of metallic

behavior even at 35 GPa, suggesting it remains a band insulator. This is attributed to the filled 4d orbitals of the heavy Cd²⁺ cation, which minimize electron correlation effects from Coulomb repulsion. Notably, the bandgap of CdPS₃ closes at a rate of approximately −30 meV/GPa, much slower than in other MPS₃ materials, indicating a higher energy scale for gap closure. This behavior, supported by observations of a piezochromic effect, further confirms CdPS₃’s band insulating nature. Overall, our study deepens the understanding of symmetry evolution and distinguishes band insulator behavior from Mott-like characteristics in CdPS₃.

SUPPLEMENTARY MATERIAL

The [supplementary material](#) contains a detailed explanation of the x-ray diffraction analysis of the CdPS₃ and the assignment of vibrational modes, symmetries, and displacement patterns under ambient conditions; additional data on the vibrational properties of CdPS₃ under compression, along with confirmation of reversibility under pressure cycle; first-principle calculation of the bandgap, volume, and enthalpies; experimental determination of the optical bandgap; and comparison of calculated phonon modes in the $R\bar{3}$ and $P\bar{3}1m$ space groups.

ACKNOWLEDGMENTS

Work at Tennessee (S.S., B.T., Y.G., K.A.S. and J.L.M.) is supported by Physical Behavior of Materials, Basic Energy Sciences, U.S. Department of Energy (Contract No. DE-SC0023144). D.M. and M.C. acknowledge funding from the Gordon and Betty Moore Foundation’s EPiQS Initiative, Grant No. GBMF9069. H.-S.K. and S.C. are supported by the Basic Science Research Program through the National Research Foundation of Korea funded by the Ministry of Science and ICT (MSIT) (Grant Nos. NRF-2020R1C1C1005900 and RS-2023-00220471). X-ray diffraction was performed at the Institute for Advanced Materials & Manufacturing (IAMM) Diffraction Facility at the University of Tennessee. Work at the National Synchrotron Light Source II at Brookhaven National Laboratory is funded by the Department of Energy (No. DE-AC98-06CH10886). Use of the 22-IR-1 beamline is supported by the National Science Foundation Division of Earth Sciences (EAR) SEES: Synchrotron Earth and Environmental Science (No. EAR- 2223273) and Chicago/DOE Alliance Center (CDAC) (No. DE-NA-0004153).

AUTHOR DECLARATIONS

Conflict of Interest

The authors have no conflicts to disclose.

Author Contributions

Sambridhi Shah: Conceptualization (equal); Data curation (equal); Formal analysis (lead); Investigation (lead); Methodology (lead); Visualization (equal); Writing – original draft (lead); Writing – review & editing (equal). **Seongjae Choi:** Software (equal); Writing – review & editing (equal). **Kevin A. Smith:** Data curation (equal);

23 July 2025 17:03:22

Methodology (equal); Supervision (equal); Validation (equal); Visualization (equal); Writing – review & editing (equal). **Yan-hong Gu:** Data curation (equal); Methodology (equal); Supervision (equal); Validation (equal); Writing – review & editing (equal). **Brian Taylor:** Investigation (supporting); Methodology (equal); Writing – review & editing (supporting). **Matthew Cothrine:** Methodology (equal); Writing – review & editing (equal). **David Mandrus:** Methodology (equal); Supervision (equal); Writing – review & editing (equal). **Zhenxian Liu:** Methodology (equal); Supervision (equal); Validation (equal); Writing – review & editing (equal). **Heung-Sik Kim:** Conceptualization (equal); Data curation (equal); Software (equal); Validation (equal); Visualization (equal); Writing – review & editing (equal). **Janice L. Musfeldt:** Conceptualization (equal); Data curation (equal); Funding acquisition (equal); Methodology (equal); Resources (equal); Supervision (equal); Validation (equal); Visualization (equal); Writing – original draft (equal); Writing – review & editing (equal).

DATA AVAILABILITY

The data that support the findings of this study are available from the corresponding authors upon reasonable request.

REFERENCES

- M. A. Susner, M. Chyasnachyus, M. A. McGuire, P. Ganesh, and P. Maksymovych, “Metal thio- and selenophosphates as multifunctional van der Waals layered materials,” *Adv. Mater.* **29**, 1602852 (2017).
- K. S. Burch, D. Mandrus, and J.-G. Park, “Magnetism in two-dimensional van der Waals materials,” *Nature* **563**, 47–52 (2018).
- T. Matsuoka, H.-S. Kim, S. Samanta, J. L. Musfeldt, and D. G. Mandrus, “ MPX_3 van der Waals magnets under pressure ($M = \text{Mn, Ni, V, Fe, Co, Cd; X = S, Se}$),” *Front. Mater.* **11**, 1362744 (2024).
- J.-G. Park, K. Zhang, H. Cheong, J. H. Kim, C. Belvin, D. Hsieh, H. Ning, and N. Gedik, “2D van der Waals magnets: from fundamental physics to applications,” *arXiv:2505.02355* (2025).
- M. J. Coak, D. M. Jarvis, H. Hamidov, C. R. S. Haines, P. L. Alireza, C. Liu, S. Son, I. Hwang, G. I. Lampronti, D. Daisenberger *et al.*, “Tuning dimensionality in van-der-Waals antiferromagnetic Mott insulators $TMPS_3$,” *J. Phys.: Condens. Matter* **32**, 124003 (2019).
- D. Tezze, J. M. Pereira, Y. Asensio, M. Ipatov, F. Calavalle, F. Casanova, A. M. Bittner, M. Ormaza, B. Martín-García, L. E. Hueso, and M. Gobbi, “Tuning the magnetic properties of $NiPS_3$ through organic-ion intercalation,” *Nanoscale* **14**, 1165–1173 (2022).
- A. Wildes, D. Lançon, M. K. Chan, F. Weickert, N. Harrison, V. Simonet, M. Zhitomirsky, M. Gvozdkova, T. Ziman, and H. Rønnow, “High field magnetization of $FePS_3$,” *Phys. Rev. B* **101**, 024415 (2020).
- S. Kang, K. Kim, B. H. Kim, J. Kim, K. I. Sim, J.-U. Lee, S. Lee, K. Park, S. Yun, T. Kim *et al.*, “Coherent many-body exciton in van der Waals antiferromagnet $NiPS_3$,” *Nature* **583**, 785–789 (2020).
- S. L. Bud’ko, E. Gati, T. J. Slade, and P. C. Canfield, “Magnetic order in the van der Waals antiferromagnet $CrPS_4$: Anisotropic H - T phase diagrams and effects of pressure,” *Phys. Rev. B* **103**, 224407 (2021).
- T. T. Mai, K. F. Garrity, A. McCreary, J. Argo, J. R. Simpson, V. Doan-Nguyen, R. V. Aguilar, and A. R. H. Walker, “Magnon-phonon hybridization in 2D antiferromagnet $MnPS_3$,” *Sci. Adv.* **7**, eabj3106 (2021).
- R. Basnet and J. Hu, “Understanding and tuning magnetism in van der Waals-type metal thiophosphates,” *Nanoscale* **16**, 15851 (2024).
- Y. Wang, J. Ying, Z. Zhou, J. Sun, T. Wen, Y. Zhou, N. Li, Q. Zhang, F. Han, Y. Xiao *et al.*, “Emergent superconductivity in an iron-based honeycomb lattice initiated by pressure-driven spin-crossover,” *Nat. Commun.* **9**, 1914 (2018).
- T. Matsuoka, A. Haglund, R. Xue, J. S. Smith, M. Lang, A. M. dos Santos, and D. Mandrus, “Pressure-induced insulator–metal transition in two-dimensional Mott insulator $NiPS_3$,” *J. Phys. Soc. Jpn.* **90**, 124706 (2021).
- M. J. Coak, D. M. Jarvis, H. Hamidov, A. R. Wildes, J. A. Paddison, C. Liu, C. R. Haines, N. T. Dang, S. E. Kichanov, B. N. Savenko *et al.*, “Emergent magnetic phases in pressure-tuned van der Waals antiferromagnet $FePS_3$,” *Phys. Rev. X* **11**, 011024 (2021).
- M. Qi, W. Chen, Y. Huang, H. Song, X. Lv, M. Wu, W. Zhao, L. Zhang, and T. Cui, “Pressure-induced superconductivity in van der Waals layered semiconductor $SnPSe_3$,” *J. Mater. Chem. C* **12**, 5108–5113 (2024).
- H. Xiang, B. Xu, Y. Xia, J. Yin, and Z. Liu, “Tunable electronic structures in MPX_3 ($M = \text{Zn, Cd; X = S, Se}$) monolayers by strain engineering,” *RSC Adv.* **6**, 89901–89906 (2016).
- F. Zhou, K. Hwangbo, Q. Zhang, C. Wang, L. Shen, J. Zhang, Q. Jiang, A. Zong, Y. Su, M. Zajac *et al.*, “Dynamical criticality of spin-shear coupling in van der Waals antiferromagnets,” *Nat. Commun.* **13**, 6598 (2022).
- Y. Gao, X. Jiang, Z. Qiu, and J. Zhao, “Photoexcitation induced magnetic phase transition and spin dynamics in antiferromagnetic $MnPS_3$ monolayer,” *npj Comput. Mater.* **9**, 107 (2023).
- R. Gusmão, Z. Sofer, and M. Pumera, “Exfoliated layered manganese trichalcogenide phosphite (MPX_3 , $X = \text{S, Se}$) as electrocatalytic van der Waals materials for hydrogen evolution,” *Adv. Funct. Mater.* **29**, 1805975 (2019).
- K.-Z. Du, X.-z. Wang, Y. Liu, P. Hu, M. I. B. Utama, C. K. Gan, Q. Xiong, and C. Kloc, “Weak van der Waals stacking, wide-range band gap, and Raman study on ultrathin layers of metal phosphorus trichalcogenides,” *ACS Nano* **10**, 1738–1743 (2016).
- S. Pei, Z. Wang, and J. Xia, “High pressure studies of 2D materials and heterostructures: A review,” *Mater. Des.* **213**, 110363 (2022).
- X. Chen, J. Wang, T. Ying, D. Huang, H. Gou, Q. Zhang, Y. Li, H. Hosono, J.-g. Guo, and X. Chen, “Insulator-metal-superconductor transition in the medium-entropy van der Waals compound $MPSe_3$ ($M = \text{Fe, Mn, Cd, and In}$) under high pressure,” *Phys. Rev. B* **106**, 184502 (2022).
- C. Haines, M. J. Coak, A. R. Wildes, G. I. Lampronti, C. Liu, P. Nahai-Williamson, H. Hamidov, D. Daisenberger, and S. S. Saxena, “Pressure-induced electronic and structural phase evolution in the van der Waals compound $FePS_3$,” *Phys. Rev. Lett.* **121**, 266801 (2018).
- N. C. Harms, T. Matsuoka, S. Samanta, A. J. Clune, K. A. Smith, A. V. Haglund, E. Feng, H. Cao, J. S. Smith, D. G. Mandrus *et al.*, “Symmetry progression and possible polar metallicity in $NiPS_3$ under pressure,” *npj 2D Mater. Appl.* **6**, 40 (2022).
- H.-S. Kim, K. Haule, and D. Vanderbilt, “Mott metal-insulator transitions in pressurized layered trichalcogenides,” *Phys. Rev. Lett.* **123**, 236401 (2019).
- D. P. Kozlenko, O. N. Lis, N. T. Dang, M. Coak, J.-G. Park, E. V. Lukin, S. E. Kichanov, N. O. Golosova, I. Y. Zel, and B. N. Savenko, “High-pressure effects on structural, magnetic, and vibrational properties of van der Waals antiferromagnet MPX_3 ,” *Phys. Rev. Mater.* **8**, 024402 (2024).
- N. C. Harms, H.-S. Kim, A. J. Clune, K. A. Smith, K. R. O’Neal, A. V. Haglund, D. G. Mandrus, Z. Liu, K. Haule, D. Vanderbilt, and J. L. Musfeldt, “Piezochromism in the magnetic chalcogenide $MnPS_3$,” *npj Quantum Mater.* **5**, 56 (2020).
- J. L. Musfeldt, D. G. Mandrus, and Z. Liu, “Insulator–metal transition in $CrSiTe_3$ triggered by structural distortion under pressure,” *npj 2D Mater. Appl.* **7**, 28 (2023).
- M. H. Whangbo, R. Brec, G. Ouvrard, and J. Rouxel, “Reduction sites of transition-metal phosphorus trichalcogenides MPX_3 ,” *Inorg. Chem.* **24**, 2459–2461 (1985).
- F. Wang, T. A. Shifa, P. Yu, P. He, Y. Liu, F. Wang, Z. Wang, X. Zhan, X. Lou, F. Xia, and J. He, “New frontiers on van der Waals layered metal phosphorous trichalcogenides,” *Adv. Funct. Mater.* **28**, 1802151 (2018).
- T. Sekine, A. Ohmamiuda, Y. Tanokura, C. Makimura, and K. Kurosawa, “Raman-scattering study of structural phase transition in layered compound $CdPS_3$,” *J. Phys. Soc. Jpn.* **62**, 800–807 (1993).
- A. Kuzmin, “First-principles LCAO study of the low- and room-temperature phases of $CdPS_3$,” *Low Temp. Phys.* **46**, 1217–1222 (2020).

- ³³M. Niu, H. Cheng, X. Li, J. Yu, X. Yang, Y. Gao, R. Liu, Y. Cao, K. He, X. Xie *et al.*, “Pressure-induced phase transitions in weak interlayer coupling CdPS₃,” *Appl. Phys. Lett.* **120**, 233104 (2022).
- ³⁴Y. Li, Y. Liu, Y. Liu, Q. Zhang, N. Su, X. Liu, J. Sun, N. Xiao, H. Liu, and Y. Li, “Pressure-induced phase transition and electronic properties of CdPX₃ (X = S and Se) by first-principles calculation,” *J. Mater. Sci.* **58**, 16144–16159 (2023).
- ³⁵S. Rahman, H. Ngyuen, D. Macdonald, and Y. Lu, “Temperature-dependent phase variations in van der Waals CdPS₃ revealed by Raman spectroscopy,” *Symmetry* **16**, 140 (2024).
- ³⁶M. J. Coak, S. Son, D. Daisenberger, H. Hamidov, C. R. S. Haines, P. L. Alireza, A. R. Wildes, C. Liu, S. S. Saxena, and J.-G. Park, “Isostructural Mott transition in 2D honeycomb antiferromagnet V_{0.9}PS₃,” *npj Quantum Mater.* **4**, 38 (2019).
- ³⁷M. Kim, H.-S. Kim, K. Haule, and D. Vanderbilt, “Orbital-selective Mott phase and non-Fermi liquid in FePS₃,” *Phys. Rev. B* **105**, L041108 (2022).
- ³⁸Y. Zhang, Y. Zhao, C. Bao, Y. Xiao, Y. Xiang, M. Song, W. Huang, L. Ma, H. Hou, and X. Chen, “Facile synthesis of cadmium phosphorus trisulfide nanosheets for highly efficient photocatalytic performance,” *J. Alloys Compd.* **909**, 164731 (2022).
- ³⁹L. D. Whittig and W. R. Allardice, “X-ray diffraction techniques,” *Methods of Soil Analysis: Part 1 Physical and Mineralogical Methods* (Soil Science Society of America, American Society of Agronomy, 1986), Vol. 5, pp. 331–362.
- ⁴⁰H. K. Mao, J. Xu, and P. M. Bell, “Calibration of the ruby pressure gauge to 800 kbar under quasi-hydrostatic conditions,” *J. Geophys. Res.: Solid Earth* **91**, 4673–4676, <https://doi.org/10.1029/jb091ib05p04673> (1986).
- ⁴¹J. A. Xu, H. K. Mao, and P. M. Bell, “High-pressure ruby and diamond fluorescence: Observations at 0.21 to 0.55 terapascal,” *Science* **232**, 1404–1406 (1986).
- ⁴²S. Ivantchev, E. Kroumova, G. Madariaga, J. M. Pérez-Mato, and M. I. Aroyo, “SUBGROUPGRAPH: A computer program for analysis of group-subgroup relations between space groups,” *J. Appl. Crystallogr.* **33**, 1190–1191 (2000).
- ⁴³G. Kresse and J. Hafner, “Ab initio molecular dynamics for liquid metals,” *Phys. Rev. B* **47**, 558–561 (1993).
- ⁴⁴G. Kresse and J. Furthmüller, “Efficient iterative schemes for ab initio total-energy calculations using a plane-wave basis set,” *Phys. Rev. B* **54**, 11169–11186 (1996).
- ⁴⁵J. P. Perdew, A. Ruzsinszky, G. I. Csonka, O. A. Vydrov, G. E. Scuseria, L. A. Constantin, X. Zhou, and K. Burke, “Restoring the density-gradient expansion for exchange in solids and surfaces,” *Phys. Rev. Lett.* **100**, 136406 (2008).
- ⁴⁶J. W. Furness, A. D. Kaplan, J. Ning, J. P. Perdew, and J. Sun, “Accurate and numerically efficient r²SCAN meta-generalized gradient approximation,” *J. Phys. Chem. Lett.* **11**, 8208–8215 (2020).
- ⁴⁷A. V. Krukau, O. A. Vydrov, A. F. Izmaylov, and G. E. Scuseria, “Influence of the exchange screening parameter on the performance of screened hybrid functionals,” *J. Chem. Phys.* **125**, 224106 (2006).
- ⁴⁸A. Togo, L. Chaput, T. Tadano, and I. Tanaka, “Implementation strategies in phonopy and phono3py,” *J. Phys.: Condens. Matter* **35**, 353001 (2023).
- ⁴⁹A. Togo, “First-principles phonon calculations with phonopy and phono3py,” *J. Phys. Soc. Jpn.* **92**, 012001 (2023).
- ⁵⁰J. Covino, P. Dragovich, C. K. Lowe-Ma, R. F. Kubin, and R. W. Schwartz, “Synthesis and characterization of stoichiometric CdPS₃,” *Mater. Res. Bull.* **20**, 1099–1107 (1985).
- ⁵¹K. Momma and F. Izumi, “VESTA 3 for three-dimensional visualization of crystal, volumetric and morphology data,” *J. Appl. Crystallogr.* **44**, 1272–1276 (2011).
- ⁵²M. I. Aroyo, J. M. Perez-Mato, D. Orobengoa, E. Tasci, G. de la Flor, and A. Kirov, “Crystallography online: Bilbao crystallographic server,” *Bulg. Chem. Commun.* **43**, 183–197 (2011).
- ⁵³E. Kroumova, M. I. Aroyo, J. M. Perez-Mato, A. Kirov, C. Capillas, S. Ivantchev, and H. Wondratschek, “Bilbao crystallographic server: Useful databases and tools for phase-transition studies,” *Phase Transitions* **76**, 155–170 (2003).
- ⁵⁴L. Kong and G. Liu, “Synchrotron-based infrared microspectroscopy under high pressure: An introduction,” *Matter Radiat. Extremes* **6**, 068202 (2021).
- ⁵⁵L. J. Langston, A. M. Ruiz, C. Boix-Constant, S. Mañas-Valero, E. Coronado, J. J. Baldoví, Z. Liu, and J. L. Musfeldt, “Pressure-induced structural phase transitions in CrSBr,” *npj Quantum Mater.* **10**, 57 (2025).
- ⁵⁶T. Matsuoka, R. Rao, M. A. Susner, B. S. Conner, D. Zhang, and D. Mandrus, “Pressure-induced insulator-to-metal transition in the van der Waals compound CoPS₃,” *Phys. Rev. B* **107**, 165125 (2023).
- ⁵⁷N. C. Harms, K. A. Smith, A. V. Haglund, D. G. Mandrus, Z. Liu, H.-S. Kim, and J. L. Musfeldt, “Metal site substitution and role of the dimer on symmetry breaking in FePS₃ and CrPS₄ under pressure,” *ACS Appl. Electron. Mater.* **4**, 3246–3255 (2022).
- ⁵⁸D. Sen and T. Saha-Dasgupta, “Pressure-tuned valence transition, insulator-metal transition in van der Waals antiferromagnet CrPS₃,” *Phys. Rev. Mater.* **7**, 064008 (2023).
- ⁵⁹Z. Liu, D. Li, Y. Liu, T. Cui, F. Tian, and D. Duan, “Metallic and anti-metallic properties of strongly covalently bonded energetic AlN₅ nitrides,” *Phys. Chem. Chem. Phys.* **21**, 12029–12035 (2019).
- ⁶⁰C. F. Matta, P. W. Ayers, and R. Cook, “The physics of electron localization and delocalization,” in *Electron Localization-Delocalization Matrices* (Springer, 2024), pp. 7–20.
- ⁶¹M. Ríflíková, R. Martoňák, and E. Tosatti, “Pressure-induced gap closing and metallization of MoSe₂ and MoTe₂,” *Phys. Rev. B* **90**, 035108 (2014).
- ⁶²M. I. Aroyo, J. M. Perez-Mato, C. Capillas, E. Kroumova, S. Ivantchev, G. Madariaga, A. Kirov, and H. Wondratschek, “Bilbao crystallographic server: I. Databases and crystallographic computing programs,” *Z. Kristallogr. Cryst. Mater.* **221**, 15–27 (2006).
- ⁶³J. L. Musfeldt, S. Singh, S. Fan, Y. Gu, X. Xu, S.-W. Cheong, Z. Liu, D. Vanderbilt, and K. M. Rabe, “Structural phase purification of bulk HfO₂: Y through pressure cycling,” *Proc. Natl. Acad. Sci. U. S. A* **121**, e2312571121 (2024).
- ⁶⁴B. Yue, W. Zhong, T. Wen, Y. Wang, H. Yu, X. Yu, C. Chen, J.-T. Wang, and F. Hong, “Pressure-induced ferroelectric-to-superconductor transition in SnPS₃,” *Phys. Rev. B* **107**, L140501 (2023).